Vibration and Buckling Characteristics of Nonlocal Beam Placed in a Magnetic Field Embedded in Winkler-Pasternak Elastic Foundation Using a New Refined Beam Theory: An Analytical approach

Subrat Kumar Jena[1], S. Chakraverty[2]*, Mohammad Malikan[3]

[1, 2]Department of Mathematics, National Institute of Technology Rourkela, 769008, India

[3]Department of Mechanics of Materials and Structures, Faculty of Civil and Environmental Engineering, Gdansk University of Technology, Gdansk, Poland

*Corresponding author

E-mail: [1]sjena430@gmail.com, [2]sne_chak@yahoo.com, [3]mohammad.malikan@pg.edu.pl

Abstract

In this article, a new refined beam theory namely one variable first-order shear deformation theory has been employed to study the vibration and buckling characteristics of nonlocal beam. The beam is exposed to an axial magnetic field and embedded in Winkler-Pasternak foundation. The Von Kármán hypothesis along with Hamilton's principle have been implemented to derive the governing equations for both the vibration and buckling studies and closed form solutions are obtained for simply supported beam using the Navier's approach. Further, a parametric study has been conducted to explore the impacts of small scale parameter, Winkler modulus, shear modulus, and magnetic field intensity on natural frequencies and critical buckling loads.

Keywords

Refined beam theory; Dynamical characteristics; Winkler-Pasternak foundation; Axial magnetic field; Navier's approach.

1. Introduction

The nanotubes were one of the first real nanomaterials to be produced at the molecular level by engineering methods. The nanotubes can be classified into different kinds of nanostructures, such as carbon nanotubes [1] (single-walled, double-walled, etc.), boron-nitride nanotubes [2] and etc. Carbon nanotubes (CNTs) made of carbon sheets with the thickness of an atom and in the shape of a hollow cylindrical, were discovered by Iijima [3]. The supernatural properties are assigned to carbon nanotubes. Among these properties, excellent flexibility, tensile strength, thermal stability and magnetic characteristics, are features that dream up predictions of nanotechnology products such as: microscopic robots, smooth and high strength bodies for automobiles, artificial arms and earthquake-resistant buildings.
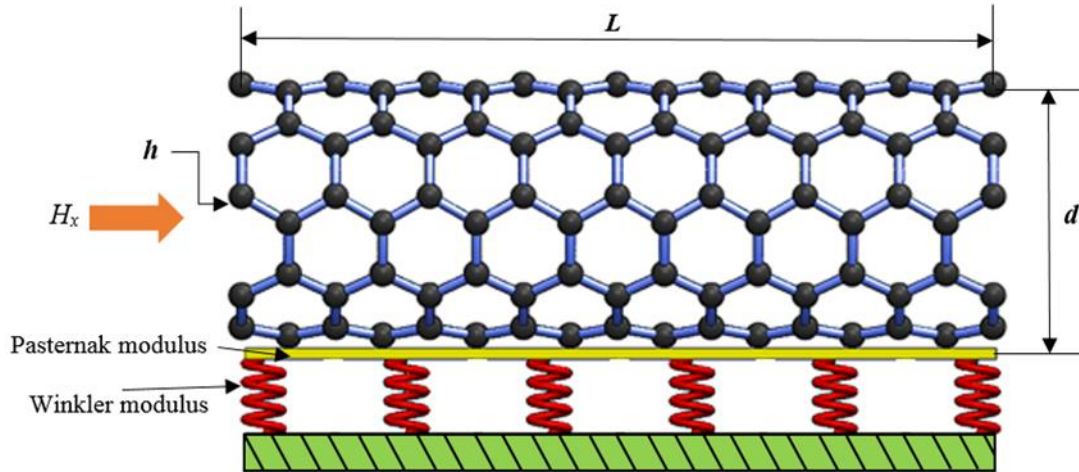

Fig. 1. The SWCNT under an axial magnetic field bridged on the Winkler-Pasternak medium

Regarding the aforementioned amazing features of the CNTs, a lot of research have been reported on these nanostructures. Therefore, it is very essential to analyze and understand the mechanical behavior of the manufactured nano parts. Due to different properties of the nanomaterials in a nanoscale against macroscale, these materials are important to be analyzed in a size-dependent scale. To consider these structures in a size-dependent domain, there are some models. Among these models, nonlocal continuum elasticity is most well-known one. Nonlocal theory of Eringen tells about nonlocality which considers a large interaction between atoms and leads to softening (decreasing stress at increasing strain). This model also is named as second stress gradient one. A lot of research have been reported on the CNTs structures based on nonlocal elasticity theory.

Murmu *et al* [4] studied the external magnetic influences on the transverse vibrations of double-walled carbon nanotubes (DWCNTs) based on the Euler-Bernoulli beam equation and elasticity theory of nonlocal. Their results proved that the increase of the magnetic effect increased the transverse natural frequencies of the nanotubes. Kiani [5] analyzed a longitudinal magnetic field affected the transverse natural frequencies of a DWCNT. The nanotubes system was bridged on a polymer foundation. The model was solved on the basis of the higher-order and Timoshenko beam approaches. Nonlocal elasticity was also utilized to simulate the interaction between atoms in a small scale. The numerical results were computed based on the several edge conditions i.e. pivot-pivot, clamped-clamped, pivot-clamped and also clamped-free. Further, Kiani [6] examined buckling and vibrations of a carbon nanotube with one wall only (SWCNT) subjected a three-dimensional magnetic field. The nonlocal continuum theory was combined with the Rayleigh beam technique to derive the equations of motion. Güven [7] investigated transverse natural frequencies of a SWCNT in a magnetic field assuming initial stress. The beam hypothesis was based on the Timoshenko one and the size-dependent behavior was modelled based on the gradient elasticity. The results were numerically shown about simple-simple edge conditions. Ponnusamy and Amuthalakshmi [8] considered the effects of magnetic and temperature of the surrounds on the natural frequencies of a nonlocal DWCNT. The Timoshenko beam hypothesis was mixed by the nonlocal theory of Eringen in order to formulate the nonlocal equations of motion. The acquired equations of motion were analytically calculated on the basis of pivot-pivot edge conditions. Zhang and Shen [9] dynamically examined a SWCNT placed into a visco-Pasternak matrix subjected to an axial magnetic field. The nanotube was in a horn-shaped model and The Euler-Bernoulli hypothesis was base of the achieved equations. The transfer function method and perturbation technique were taken to calculate the numeric vibration modes. Hosseini and Sadeghi-Goughari [10] presented the buckling modes and natural frequencies of a nanotube under an axial magnetic field conveying fluid. Differential transformation method was stood for giving the numeric outcomes. Their best results proved that the axial magnetic field increased natural frequencies and the flow velocity. Nonlinear natural frequencies of a SWCNT subjected to a magnetic field with random material features using nonlinear damping was studied by Chang [11]. Kiani [12] with assuming the existence of an axial magnetic field dynamically analyzed the periodic arrays of SWCNTs in the thermal environment based on the stress nonlocality. Moreover, Zhen *et al* [13] based on the viscoelasticity properties of the SWCNTs, higher-order beam hypothesis and nonlocal

3

strain gradient model, studied the natural frequencies of a nanotube. To the sake of the brevity, the other important research done on the carbon nanotubes and nanobeam are found by [14-42].

Civalek and Demir [43] studied buckling and bending characteristics of cantilever carbon nanotube using Euler-Bernoulli beam theory, and the small scale effects of the CNT was captured by Eringen's elasticity theory. Li *et al* [44] employed analytical approach and finite element method to investigate the longitudinal vibration of rods using a nonlocal strain gradient model. Barretta *et al* [45] investigated higher order version of Eringen's model using Euler-Bernoulli beam. Implementation of integral form of nonlocal Euler Bernoulli beam for the dynamic response analysis was studied by Eptaimeros *et al* [46]. Rahmani *et al* [47] implemented Navier's approach to study bending and buckling of FGM beam using several nonlocal higher order shear deformation beam theories. Akgoz and Civalek [48] applied both the hyperbolic shear deformation and modified couple stress theories to analyze the effects of thermal and shear deformation on the vibrational behavior of functionally graded microbeam. Mercan and Civalek [49] investigated buckling behavior of Silicon carbide nanotubes considering the surface effect and small scale effect using harmonic differential quadrature method. Demir and Civalek [50] used enhanced Eringen differential model to study bending of micro beams under the framework of Euler-Bernoulli beam theory. Some other pioneering works by different researchers can been seen in [51-55].

Carbon nanotubes and nanobeams with magnetic property can present many applications in engineering. As an example, in order to separate pollutants like heavy metals, dangerous organic and mineral compounds from water solotions, the tubes have attracted the attention of scientists. To this, with making a magnetic field around the nanobeams placed in a polluted environment, all of the above-mentioned pollutants can be absorbed to the nanobeams leading to a safe and healthy water [56, 57]. Inevitably, the magnetic field can affect the nanobeam and hence results in mechanical reaction of the nanobeam. In fact, the CNTs may not give researchers a good performance to absorb the pollutants if they do not know about mechanical response of the nanobeams in a magnetic surround. There are many other examples that can be mentioned. Therefore, in this case, deformation and resistance reaction of nanobeams in a magnetic field was as an engineering motivation for this research.

As review the crucial and the best research on the CNTs, the authors aim at the reconsidering the SWCNTs in both mechanical stability and vibrations under a longitudinal magnetic environment on the basis of a new refined beam hypothesis which can be seen in Fig. 1. The refined beam model is based on the one variable resulting in lower number of equations. To include the behavior of the nanostructure at its real domain, the continuous nonlocal theory is employed. Furthermore, a well-known elastic foundation, namely Winkler-Pasternak, is located under the nanotube in order to find the nanotube more stable. The Navier analytical technique is base of the numerical findings for a pivot-pivot edge condition. After all, the deeply considerations are shown for key parameters such as, magnetic effect, small scale impacts and the foundations influences.

2. Proposed model

From Maxwell's Electromagnetic equations, we have [58-60]

$$
\nabla \times H = \frac{\partial D}{\partial t} + J, \quad \nabla \times E = -B
$$
$$
\nabla D = \rho_b, \quad \nabla B = 0 \tag{1}
$$
$$
D = \varepsilon E, \quad B = \eta H
$$

In which (ρ_b) is the static charge density, (E) is the electric field intensity, (H) is the magnetic field intensity, (J) is the current density vector, (B) is the magnetic field density, (D) is the displacement current density, ε and η are the electric and magnetic permeability of the beam, respectively. Now, by neglecting the displacement current density and considering the small disturbances of the initially applied electromagnetic field as $e = e(x, y, z, t)$ and $h = h(x, y, z, t)$, the electromagnetic fields can be represented as

$$
E = E_0 + e, \quad H = H_0 + h \tag{2}
$$

In the present investigation, we have neglected the initially applied electric field which results into $E = e$. Now, the Eq. (1) can be rewritten as [58-60]

$$
J = \nabla \times h, \quad \nabla \times e = -\eta \frac{\partial h}{\partial t}
$$
$$
\nabla h = 0, \quad e = -\eta \left(\frac{\partial u}{\partial t} \times H_0 \right) \tag{3}
$$
$$
h = \nabla \times (u \times H_0)
$$

Here $u = (u, 0, w)$ represents the displacement field vector of the beam. Considering only axial magnetic field as $H = (H_x, 0, 0)$ acting on the beam, we obtain

$$h = -H_x \left(\frac{\partial v}{\partial y} + \frac{\partial w}{\partial z} \right) i + H_x \frac{\partial v}{\partial x} j + H_x \frac{\partial w}{\partial x} k \tag{4}$$

The Lorentz force induced by the axial magnetic field is computed as [58-60]

$$f = \eta (J \times H) = \eta \left[H_x^2 \left(\frac{\partial^2 v}{\partial x^2} + \frac{\partial^2 v}{\partial y^2} + \frac{\partial^2 w}{\partial y \partial z} \right) j + H_x^2 \left(\frac{\partial^2 w}{\partial x^2} + \frac{\partial^2 w}{\partial y^2} + \frac{\partial^2 v}{\partial y \partial z} \right) k \right] \tag{5}$$

Likewise, the resultant Lorentz force can be obtained as [58-60]

$$f_{Lz} = \eta \int_A f_z dA = \eta A H_x^2 \frac{\partial^2 w}{\partial x^2} \tag{6}$$

The displacement fields, as per new refined beam theory can be expressed as [20, 21, 27]

$$u_1(x,z,t) = u(x,t) - z \frac{\partial w(x,t)}{\partial x}$$
$$u_2(x,z,t) = 0 \tag{7}$$
$$u_3(x,z,t) = w(x,t) + B \frac{\partial^2 w}{\partial x^2}$$

In which $u(x,t)$ and $w(x,t)$ are the displacements of the neutral axis in axial and transverse directions, respectively. $B = \frac{EI}{AG}$, where E is the Young's modulus, $I = \int_A z^2 \, dA$ is the moment of area, A is the area of cross-section, and G is the shear modulus. Considering Von Kármán hypothesis, the strain displacement relations are given as

$$\varepsilon_{xx} = \frac{\partial u}{\partial x} - z \frac{\partial^2 w}{\partial x^2} + \frac{1}{2} \left(B \frac{\partial^3 w}{\partial x^3} + \frac{\partial w}{\partial x} \right)^2$$
$$\gamma_{xz} = B \frac{\partial^3 w}{\partial x^3} \tag{8}$$

The virtual strain energy (δU) may be written as

6

$$\delta U = \iiint_V \left(\sigma_{xx} \delta \varepsilon_{xx} + \sigma_{xz} \delta \gamma_{xz} \right) dV$$

$$= \int_0^L \left[\begin{array}{l} N_{xx} \dfrac{\partial \delta u}{\partial x} - M_{xx} \dfrac{\partial^2 \delta w}{\partial x^2} + Q_{xz} B \dfrac{\partial^3 \delta w}{\partial x^3} + \\[2mm] N_{xx} \left(B^2 \dfrac{\partial^3 w}{\partial x^3} \dfrac{\partial^3 \delta w}{\partial x^3} + B \dfrac{\partial^3 w}{\partial x^3} \dfrac{\partial \delta w}{\partial x} + B \dfrac{\partial w}{\partial x} \dfrac{\partial^3 \delta w}{\partial x^3} + \dfrac{\partial w}{\partial x} \dfrac{\partial \delta w}{\partial x} \right) \end{array} \right] dx \qquad (9)$$

$$= \int_0^L \left[\begin{array}{l} -\dfrac{\partial N_{xx}}{\partial x} \delta u + \dfrac{\partial^2 M_{xx}}{\partial x^2} \delta w - B \dfrac{\partial^3 Q_{xz}}{\partial x^3} \delta w - B^2 \left(\dfrac{\partial^3}{\partial x^3} \left(N_{xx} \dfrac{\partial^3 w}{\partial x^3} \right) \right) \delta w \\[3mm] - B \left(\dfrac{\partial}{\partial x} \left(N_{xx} \dfrac{\partial^3 w}{\partial x^3} \right) \right) \delta w - B \left(\dfrac{\partial^3}{\partial x^3} \left(N_{xx} \dfrac{\partial w}{\partial x} \right) \right) \delta w - \dfrac{\partial}{\partial x} \left(N_{xx} \dfrac{\partial w}{\partial x} \right) \delta w \end{array} \right] dx$$

where $M_{xx} = \int_A z \sigma_{xx} dA$, $N_{xx} = \int_A \sigma_{xx} dA$, and $Q_{xz} = \int_A \sigma_{xz} dA$ are the local stress resultants of the beam. The kinetic energy (T) of the beam can be written as

$$T = \frac{1}{2} \rho \iiint_v \left[\left(\frac{\partial u_1}{\partial t} \right)^2 + \left(\frac{\partial u_3}{\partial t} \right)^2 \right] dV \qquad (10)$$

Now the virtual kinetic energy (δT) can be computed as

$$\delta T = \int_0^L \left[\begin{array}{l} I_0 \dfrac{\partial u}{\partial t} \dfrac{\partial \delta u}{\partial t} + I_2 \dfrac{\partial^2 w}{\partial x \partial t} \dfrac{\partial^2 \delta w}{\partial x \partial t} + I_0 \dfrac{\partial w}{\partial t} \dfrac{\partial \delta w}{\partial t} + \\[3mm] I_0 B \dfrac{\partial w}{\partial t} \dfrac{\partial^3 \delta w}{\partial x^2 \partial t} + I_0 B \dfrac{\partial^3 w}{\partial x^2 \partial t} \dfrac{\partial \delta w}{\partial t} + I_0 B^2 \dfrac{\partial^3 w}{\partial x^2 \partial t} \dfrac{\partial^3 \delta w}{\partial x^2 \partial t} \end{array} \right] dx \qquad (11)$$

$$= \int_0^L \left[-I_0 \frac{\partial^2 u}{\partial t^2} \delta u - \left(I_2 \frac{\partial^4 w}{\partial x^2 \partial t^2} + I_0 \frac{\partial^2 w}{\partial t^2} + 2 I_0 B \frac{\partial^4 w}{\partial x^2 \partial t^2} + B^2 I_0 \frac{\partial^6 w}{\partial x^4 \partial t^2} \right) \delta w \right] dx$$

In which $I_0 = \rho A$ and $I_2 = \rho I$, are called mass moments of inertia.

The virtual work done (δW) by external loads is defined as

$$\delta W = \int_0^L \left[\left(\eta A H_x^2 \right) \left(\frac{\partial^2 w}{\partial x^2} \right) - k_w w + k_p \left(\frac{\partial^2 w}{\partial x^2} \right) \right] \delta w \, dx, \qquad (12)$$

where k_w is the Winkler modulus, k_p is the shear modulus, η is the magnetic permeability, and H_x is the strength of axial magnetic field.

7

Using Hamilton's principle $\delta \Pi = \int_0^t \delta \left(T - \left(U + W \right) \right) dt,$ we obtain the equations of motion as

$$\frac{\partial N_{xx}}{\partial x} = I_0 \frac{\partial^2 u}{\partial t^2} \tag{13}$$

$$\left[\begin{array}{c} -\frac{\partial^2 M_{xx}}{\partial x^2} + B \frac{\partial^3 Q_{xz}}{\partial x^3} + B^2 \left(\frac{\partial^3}{\partial x^3} \left(N_{xx} \frac{\partial^3 w}{\partial x^3} \right) \right) + B \left(\frac{\partial}{\partial x} \left(N_{xx} \frac{\partial^3 w}{\partial x^3} \right) \right) + \\ B \left(\frac{\partial^3}{\partial x^3} \left(N_{xx} \frac{\partial w}{\partial x} \right) \right) + \frac{\partial}{\partial x} \left(N_{xx} \frac{\partial w}{\partial x} \right) - \left(\eta A H_x^2 \right) \left(\frac{\partial^2 w}{\partial x^2} \right) + k_w w - \\ k_p \left(\frac{\partial^2 w}{\partial x^2} \right) - I_2 \frac{\partial^4 w}{\partial x^2 \partial t^2} - I_0 \left(\frac{\partial^2 w}{\partial t^2} + 2B \frac{\partial^4 w}{\partial x^2 \partial t^2} + B^2 \frac{\partial^6 w}{\partial x^4 \partial t^2} \right) \end{array} \right] = 0 \tag{14a}$$

The Eq. (14a) is further simplified as

$$\left[\begin{array}{c} -\frac{\partial^2 M_{xx}}{\partial x^2} + B \frac{\partial^3 Q_{xz}}{\partial x^3} + N_{xx} \left(B^2 \frac{\partial^6 w}{\partial x^6} + 2B \frac{\partial^4 w}{\partial x^4} + \frac{\partial^2 w}{\partial x^2} \right) - \left(\eta A H_x^2 \right) \left(\frac{\partial^2 w}{\partial x^2} \right) \\ + k_w w - k_p \left(\frac{\partial^2 w}{\partial x^2} \right) - I_2 \frac{\partial^4 w}{\partial x^2 \partial t^2} - I_0 \left(\frac{\partial^2 w}{\partial t^2} + 2B \frac{\partial^4 w}{\partial x^2 \partial t^2} + B^2 \frac{\partial^6 w}{\partial x^4 \partial t^2} \right) \end{array} \right] = 0 \tag{14b}$$

The local stress resultants, using Hookean stress-strain elasticity relation can be rewritten as

$$M_{xx} = -EI \frac{\partial^2 w}{\partial x^2}$$
$$Q_{xz} = AGB \frac{\partial^3 w}{\partial x^3} \tag{15}$$

From the Eringen's nonlocal elasticity theory [61], we have

$$\left(1 - \left(e_0 a \right)^2 \frac{\partial^2}{\partial x^2} \right) \sigma_{ij} = C_{ijkl} \varepsilon_{kl} \tag{16}$$

In which $\sigma_{ij}, \varepsilon_{kl}$ and C_{ijkl} are stress tensor, strain tensor and elastic constant, respectively.

Further, from Eq. (16), we have

$$\left(1 - \left(e_0 a \right)^2 \frac{\partial^2}{\partial x^2} \right) \sigma_{xx} = E \varepsilon_{xx} \tag{17.a}$$

$$\left(1-\left(e_0 a\right)^2 \frac{\partial^2}{\partial x^2}\right)\sigma_{xz} = 2G\varepsilon_{xz}$$ (17.b)

Employing Eq. (17), the nonlocal stress resultants may be given as

$$\left(1-\left(e_0 a\right)^2 \frac{\partial^2}{\partial x^2}\right)M_{xx} = -EI\frac{\partial^2 w}{\partial x^2}$$ (18.a)

$$\left(1-\left(e_0 a\right)^2 \frac{\partial^2}{\partial x^2}\right)Q_{xz} = AGB\frac{\partial^3 w}{\partial x^3}$$ (18.b)

Implementing Eq. (18) in Eq. (14), the governing equation of motion is expressed as

$$\left(1-\left(e_0 a\right)^2 \frac{\partial^2}{\partial x^2}\right)\begin{bmatrix} -N_{xx}\left(B^2\frac{\partial^6 w}{\partial x^6} + 2B\frac{\partial^4 w}{\partial x^4} + \frac{\partial^2 w}{\partial x^2}\right) + \left(\eta A H_x^2\right)\left(\frac{\partial^2 w}{\partial x^2}\right) - k_w w + \\ k_p\left(\frac{\partial^2 w}{\partial x^2}\right) + I_2\left(\frac{\partial^4 w}{\partial x^2 \partial t^2}\right) + I_0\left(\frac{\partial^2 w}{\partial t^2} + 2B\frac{\partial^4 w}{\partial x^2 \partial t^2} + B^2\frac{\partial^6 w}{\partial x^4 \partial t^2}\right) \end{bmatrix}$$

$$= EI\frac{\partial^4 w}{\partial x^4} + AGB^2\frac{\partial^6 w}{\partial x^6}$$ (19)

For finding the buckling load, the time derivative terms are required to be ignored and the in-plane force resultant $\left(N_{xx}\right)$ is replaced by $-P$ in Eq. (19) and the governing equation is given as

$$\left(1-\left(e_0 a\right)^2 \frac{\partial^2}{\partial x^2}\right)\begin{bmatrix} P\left(B^2\frac{\partial^6 w}{\partial x^6} + 2B\frac{\partial^4 w}{\partial x^4} + \frac{\partial^2 w}{\partial x^2}\right) + \\ \left(\eta A H_x^2\right)\left(\frac{\partial^2 w}{\partial x^2}\right) - k_w w + k_p\left(\frac{\partial^2 w}{\partial x^2}\right) \end{bmatrix} = EI\frac{\partial^4 w}{\partial x^4} + AGB^2\frac{\partial^6 w}{\partial x^6}$$ (20)

For linear free vibration, the in-plane force resultant $\left(N_{xx}\right)$ is neglected from Eq. (19) and the governing equation of motion may be stated as

$$\left(1-\left(e_0 a\right)^2 \frac{\partial^2}{\partial x^2}\right)\begin{bmatrix} \left(\eta A H_x^2\right)\left(\frac{\partial^2 w}{\partial x^2}\right) - k_w w + k_p\left(\frac{\partial^2 w}{\partial x^2}\right) + I_2\left(\frac{\partial^4 w}{\partial x^2 \partial t^2}\right) \\ + I_0\left(\frac{\partial^2 w}{\partial t^2} + 2B\frac{\partial^4 w}{\partial x^2 \partial t^2} + B^2\frac{\partial^6 w}{\partial x^4 \partial t^2}\right) \end{bmatrix} = EI\frac{\partial^4 w}{\partial x^4} + AGB^2\frac{\partial^6 w}{\partial x^6}$$ (21)

9

3. Analytical Method

In this research, Navier's method has been incorporated to study the buckling characteristics as well as vibration characteristics analytically for Simply supported- Simply supported (SS) boundary condition. The transverse displacement (w), as per Navier's approach may be expressed as [20, 21, 27]

$$w(x,t) = \sum_{n=1}^{\infty} W_n \sin\left(\frac{n\pi}{L}x\right) e^{i\omega_n t} \tag{22}$$

In which W_n, and ω_n are the displacement and frequency of the beam.

Plugging Eq. (22) in Eq. (21), the frequency parameter (ω^2) may be stated as

$$\omega_n^2 = \frac{\begin{matrix} \eta AH_x^2\left(\dfrac{n\pi}{L}\right)^2 + (e_0 a)^2 \eta AH_x^2\left(\dfrac{n\pi}{L}\right)^4 + k_w + (e_0 a)^2 k_w\left(\dfrac{n\pi}{L}\right)^2 \\[3mm] + k_p\left(\dfrac{n\pi}{L}\right)^2 + (e_0 a)^2 k_p\left(\dfrac{n\pi}{L}\right)^4 + EI\left(\dfrac{n\pi}{L}\right)^4 - AGB^2\left(\dfrac{n\pi}{L}\right)^6 \end{matrix}}{\begin{matrix}\left\langle I_2\left(\dfrac{n\pi}{L}\right)^2 - I_0 + 2BI_0\left(\dfrac{n\pi}{L}\right)^2 - B^2 I_0\left(\dfrac{n\pi}{L}\right)^4\right\rangle + (e_0 a)^2 \\[3mm] \left\langle I_2\left(\dfrac{n\pi}{L}\right)^4 - I_0\left(\dfrac{n\pi}{L}\right)^2 + 2BI_0\left(\dfrac{n\pi}{L}\right)^4 - B^2 I_0\left(\dfrac{n\pi}{L}\right)^6\right\rangle\end{matrix}} \tag{23}$$

Substituting Eq. (22) in Eq. (20), the buckling load can be obtained as

$$P_n = \frac{\begin{matrix} \eta AH_x^2\left(\dfrac{n\pi}{L}\right)^2 + (e_0 a)^2 \eta AH_x^2\left(\dfrac{n\pi}{L}\right)^4 + k_w + (e_0 a)^2 k_w\left(\dfrac{n\pi}{L}\right)^2 \\[3mm] + k_p\left(\dfrac{n\pi}{L}\right)^2 + (e_0 a)^2 k_p\left(\dfrac{n\pi}{L}\right)^4 + EI\left(\dfrac{n\pi}{L}\right)^4 - AGB^2\left(\dfrac{n\pi}{L}\right)^6 \end{matrix}}{\begin{matrix}\left\langle -B^2\left(\dfrac{n\pi}{L}\right)^6 + 2B\left(\dfrac{n\pi}{L}\right)^4 - \left(\dfrac{n\pi}{L}\right)^2\right\rangle + (e_0 a)^2 \\[3mm] \left\langle -B^2\left(\dfrac{n\pi}{L}\right)^8 + 2B\left(\dfrac{n\pi}{L}\right)^6 - \left(\dfrac{n\pi}{L}\right)^4\right\rangle\end{matrix}} \tag{24}$$

10

4. Results and discussions

The natural frequencies (ω_n) and critical buckling loads (P_1) or (P_{cr}) are calculated from Eq. (23) and Eq. (24), respectively implementing the Navier's method. In this investigation, we have considered Single Walled Carbon Nanotube (SWCNT) for the case study by using the following properties or parameters [62].

$E = 1TPa$, Poisson's ratio $(\upsilon) = 0.28$, mass density $(\rho) = 2.24\, g\,/\,cm^3$, diameter $(d) = 1.1nm$, Effective thickness $(h) = 0.342nm$, Magnetic permeability $(\eta) = 4\pi \times 10^{-7}\, H/m$, unless mentioned $L = 10$, and Magnetic field intensity $(H_x) = 4 \times 10^8\, A/m$.

4.1 Validation

The critical buckling loads (P_{cr}) and the frequency parameters $\left(\lambda = \omega L^2 \sqrt{\rho A / EI}\right)$ are validated by comparing with other published article in special cases. For the validation of critical buckling loads (P_{cr}), Winkler foundation (k_w), Pasternak foundation (k_p), and the magnetic field intensity (H_x) are set to zero and then the results are compared with [21] for different nonlocal parameters and different lengths of beam which can be depicted in Table 1. For the computational purpose we have considered $E = 1TPa$, Poisson's ratio $(\upsilon) = 0.18$, and diameter $(d) = 1nm$. Likewise to exhibit the exactness of the frequency parameters $\left(\sqrt{\lambda}\right)$, the present results are compared with [63] by neglecting Winkler foundation (k_w), Pasternak foundation (k_p), shear modulus (G), and the magnetic field intensity (H_x) which is demonstrated in Fig. 2 as graphical results. From these results, an excellent agreement can be witnessed.
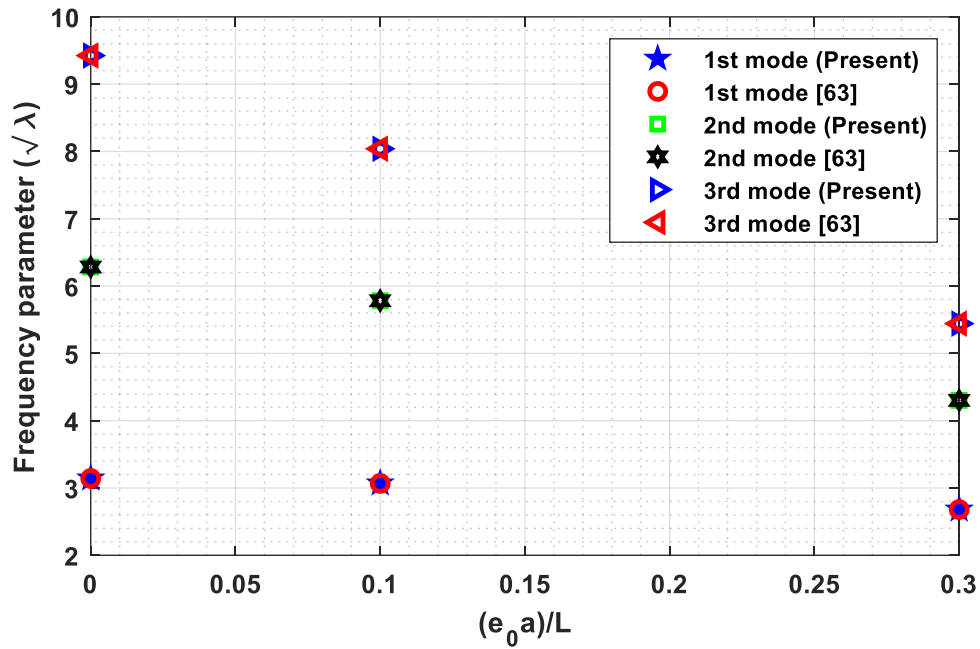
11

Fig. 2. Comparison of frequency parameters with [63]

Table 1 Validation of critical buckling load $\left(P_{cr}\right)$ with [21]

e_0a	Present					[21]				
	$L=12$	$L=14$	$L=16$	$L=18$	$L=20$	$L=12$	$L=14$	$L=16$	$L=18$	$L=20$
0	3.3991	2.4905	1.9034	1.5021	1.2156	3.3991	2.4905	1.9034	1.5021	1.2156
0.5	3.3418	2.4595	1.8852	1.4907	1.2082	3.3418	2.4595	1.8852	1.4907	1.2082
1	3.1810	2.3711	1.8327	1.4577	1.1864	3.1810	2.3711	1.8327	1.4577	1.1864
1.5	2.9449	2.2370	1.7515	1.4057	1.1517	2.9449	2.2370	1.7515	1.4057	1.1517
2	2.6677	2.0729	1.6494	1.3389	1.1064	2.6677	2.0729	1.6494	1.3389	1.1064

Additionally, Table 2 was added to improve the validity of the refined beam model presented in this paper. The numerical outcomes of Table 2 were obtained from [64] on the base of nonlocal elasticity theory. Beside the model, an inestimable comparison, namely the molecular dynamics

method (MD) is shown properly. The results of [64] was for first-order of shear deformation model in a shell domain for the carbon nanotube also for simply-supported boundary conditions. For the computational aims the $(E) = 1.06 TPa$, Poisson's ratio $(\upsilon) = 0.19$, and diameter $d = 0.68 nm$ were considered. Furthermore, the amounts of small scale factors were selected as $e_0 a = 3.3$ to $3.5 nm$. Although the numerical outcomes of nanotubes when they are assumed as a shell [64] is in a better agreement with molecular mechanics' results, a good agreement for the present beam model is also observed.

Table 2 Comparison of natural frequencies (THz) for a nanotube

L/d	[64] (MD)	Nonlocal elasticity theory	
		[64]	Present, [20]
8.47	0.466	0.333	0.354
13.89	0.190	0.165	0.163
17.47	0.122	0.121	0.124

4.2 Effect of small scale parameter

Influence of nonlocal effect on critical buckling load (P_{cr}) and natural frequency (ω) has been studied with $k_w = 1 GPa$, and $k_p = 500 nN$. For natural frequency, first four modes are taken into consideration where as critical buckling loads are calculated for different lengths of the beam. Here, nonlocal parameters $(e_0 a)$ are assumed as 0, 0.5, 1, 1.5, 2, 2.5, 3, 3.5, 4 for both the dynamic characteristics study. Likewise, lengths of the beam (L) are considered as 5, 10, 15 for buckling analysis. In this regards, Table 3 and Fig. 3 represent the tabular and graphical results for natural frequency while Table 4 and Fig. 4 epitomize for critical buckling loads. Both the natural frequencies and critical buckling loads are decreasing with the increase of nonlocal parameters. In case of vibration, higher modes are more sensitive towards the nonlocality whereas beam with small sizes possess higher critical buckling loads that exhibit remarkable response towards the small scale effect.

Table 3 Natural frequency (ω) in THz with $k_w = 1 GPa$, and $k_p = 500 nN$

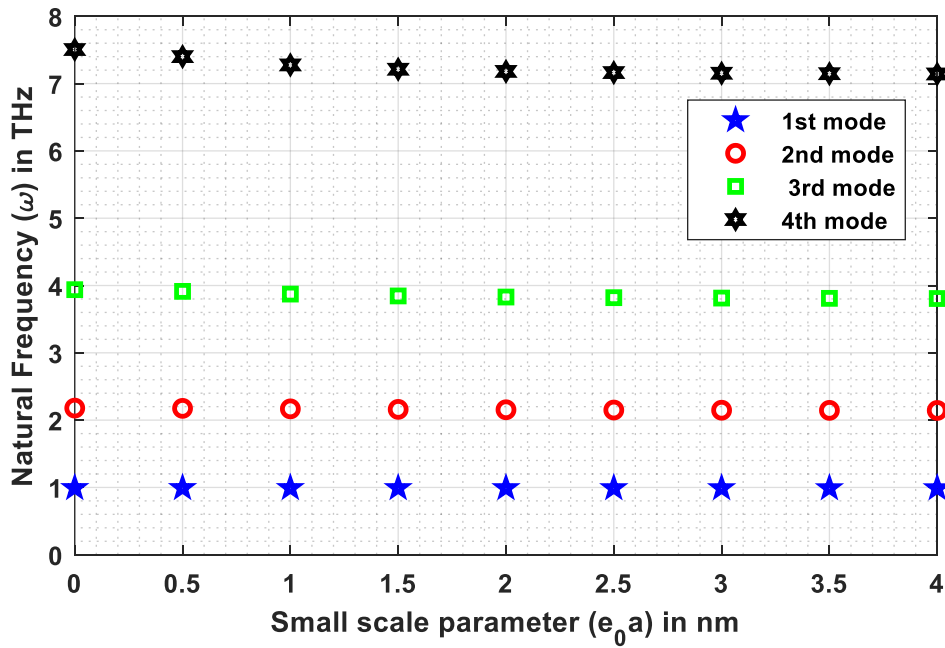| $e_0 a$ in nm	ω_1	ω_2	ω_3	ω_4
0	0.9918	2.1787	3.9382	7.5061
0.5	0.9917	2.1751	3.9130	7.4011
1	0.9914	2.1674	3.8725	7.2771
1.5	0.9909	2.1598	3.8449	7.2129
2	0.9904	2.1541	3.8287	7.1810
2.5	0.9900	2.1501	3.8192	7.1638
3	0.9895	2.1473	3.8132	7.1536
3.5	0.9891	2.1453	3.8094	7.1472
4	0.9888	2.1439	3.8067	7.1429

Fig. 3. Natural frequency Vs. Small scale parameter

14

Table 4 Critical buckling load $\left(P_{cr}\right)$ in nN with $k_w = 1GPa$, and $k_p = 500nN$

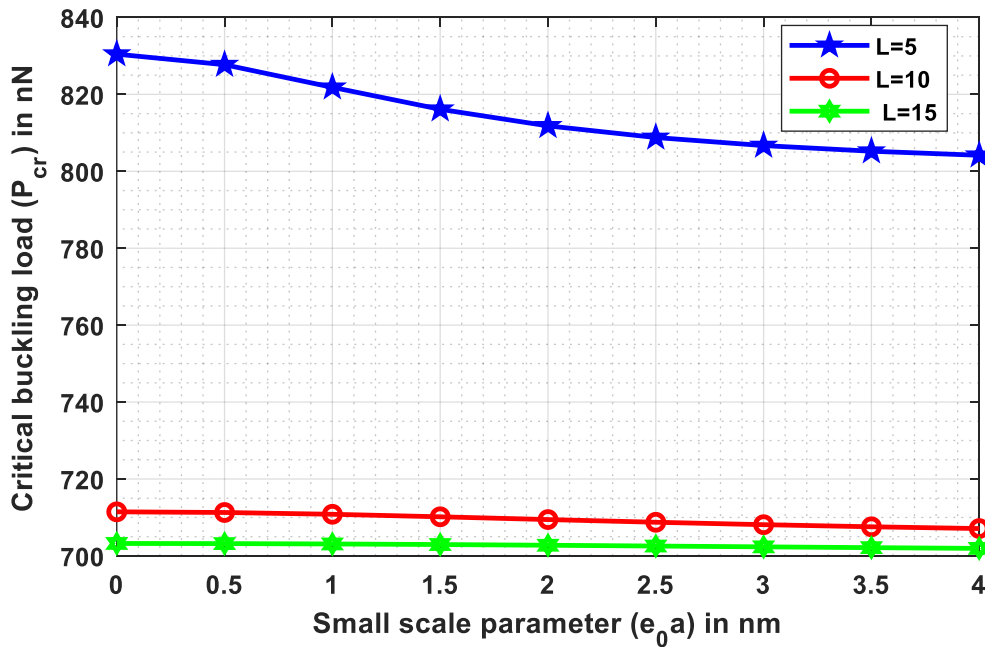| e_0a in nm	P_{cr} with $L=5$	P_{cr} with $L=10$	P_{cr} with $L=15$
0	830.4534	711.4611	703.2364
0.5	827.7178	711.2901	703.2025
1	821.8339	710.8230	703.1053
1.5	816.1280	710.1704	702.9563
2	811.8080	709.4506	702.7709
2.5	808.7832	708.7511	702.5654
3	806.6891	708.1197	702.3538
3.5	805.2186	707.5734	702.1464
4	804.1628	707.1120	701.9504

Fig. 4. Critical buckling load Vs. Small scale parameter

15

4.3 Effect of Winkler modulus

This subsection deals with the response of Winkler modulus (k_w) on dynamic characteristics of the nonlocal beam. In order to analyze the impact of k_w on natural frequency (ω), $L = 10nm$, $e_0 a = 0.5nm$, and $k_p = 500nN$ are considered. Also, k_w is taken from 0 to 5 GPa with an increment of 0.5 GPa which can be seen in Table 5 and Fig. 5 as tabular and graphical results, respectively. To study the effect of k_w on critical buckling load (P_{cr}), Winkler modulus is considered as 0, 1, 2, 3, 4, 5GPa and $k_p = 500nN$ for different values of small scale parameters which are depicted in Table 6 and Fig. 6. From this study, we may observe that natural frequencies and critical buckling loads are increasing with increase of k_w but this increase is more sharper in case of critical buckling load. Further, beam with lower value of nonlocal parameter possesses less value of critical buckling load.

Table 5 Natural frequency (ω) in THz with $L = 10nm$, $e_0 a = 0.5nm$, and $k_p = 500nN$

k_w in GPa	ω_1	ω_2	ω_3	ω_4
0	0.9843	2.1711	3.9098	7.3978
0.5	0.9880	2.1731	3.9114	7.3995
1	0.9917	2.1751	3.9130	7.4011
1.5	0.9954	2.1771	3.9145	7.4027
2	0.9991	2.1791	3.9161	7.4044
2.5	1.0027	2.1811	3.9176	7.4060
3	1.0064	2.1831	3.9192	7.4076
3.5	1.0100	2.1851	3.9207	7.4093
4	1.0136	2.1871	3.9223	7.4109
4.5	1.0172	2.1890	3.9239	7.4125
5	1.0208	2.1910	3.9254	7.4142

16

Table 6 Critical buckling load $\left(P_{cr}\right)$ in nN with $L = 10nm$, and $k_p = 500nN$

k_w in GPa	P_{cr} with $e_0a = .5$	P_{cr} with $e_0a = 1$	P_{cr} with $e_0a = 1.5$	P_{cr} with $e_0a = 2$
0	700.7004	700.2334	699.5807	698.8610
1	711.2901	710.8230	710.1704	709.4506
2	721.8797	721.4127	720.7600	720.0402
3	732.4693	732.0023	731.3496	730.6299
4	743.0590	742.5919	741.9393	741.2195
5	753.6486	753.1816	752.5289	751.8091
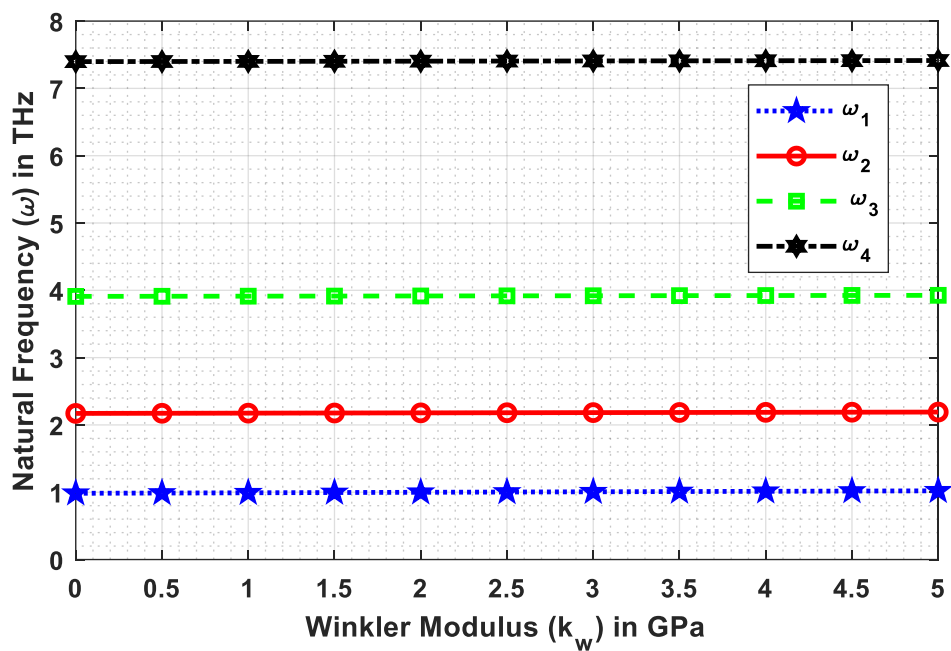
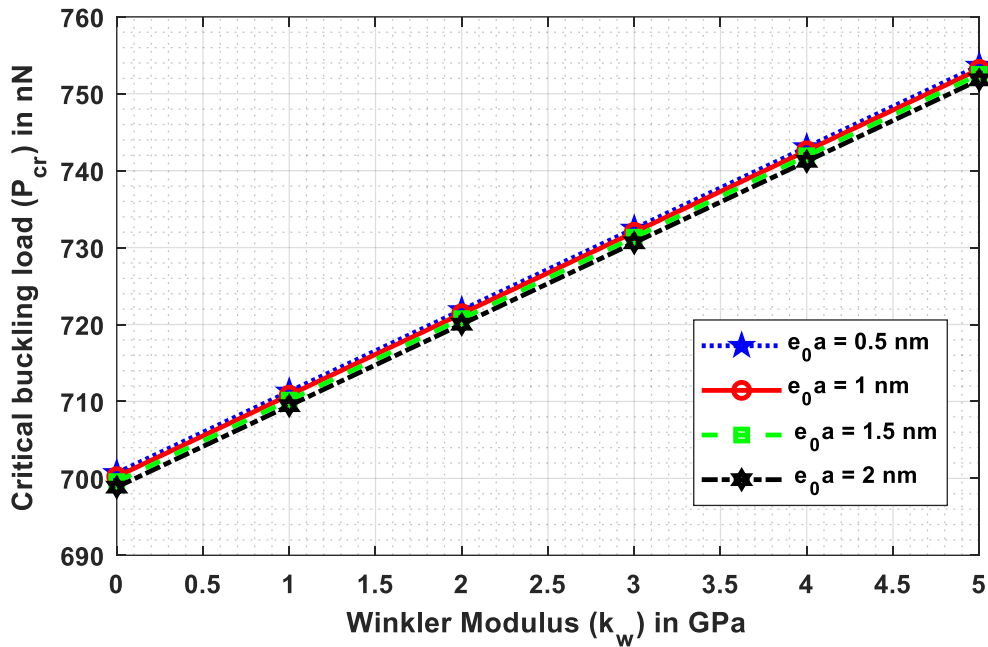**Fig. 5.** Natural frequency Vs. Winkler modulus

Fig. 6. Critical buckling load Vs. Winkler modulus

4.4 Effect of shear modulus

The impacts of shear modulus (k_p) are investigated through this subsection. The natural frequencies (ω) are noted for different values of shear modulus (0, 100, 200, 300, 400, 500nN) with $L = 10nm$, $e_0 a = 1nm$, and $k_w = 1GPa$. In this regard, Table 7 and Fig. 7 are presented to exhibit the response of (k_p) on ω. From this results, it is witnessed that the natural frequencies are increasing rapidly with the increase of k_p. Likewise, the response of shear modulus (k_p) is noted on critical buckling load for different values of shear modulus as well as different values of nonlocal parameters which are displayed in Table 8 and Fig. 8. This results reveals that the critical buckling loads increase very sharply with the rise of shear modulus (k_p).

Table 7 Natural frequency (ω) in THz with $L = 10\,nm$, $e_0 a = 1\,nm$, and $k_w = 1\,GPa$

k_p in nN	ω_1	ω_2	ω_3	ω_4
0	0.5102	1.1253	2.0380	3.8365
100	0.6362	1.3973	2.5144	4.7293
200	0.7412	1.6244	2.9139	5.4785
300	0.8330	1.8234	3.2649	6.1368
400	0.9156	2.0028	3.5816	6.7311
500	0.9914	2.1674	3.8725	7.2771

Table 8 Critical buckling load (P_{cr}) in nN with $L = 10\,nm$, and $k_w = 1\,GPa$

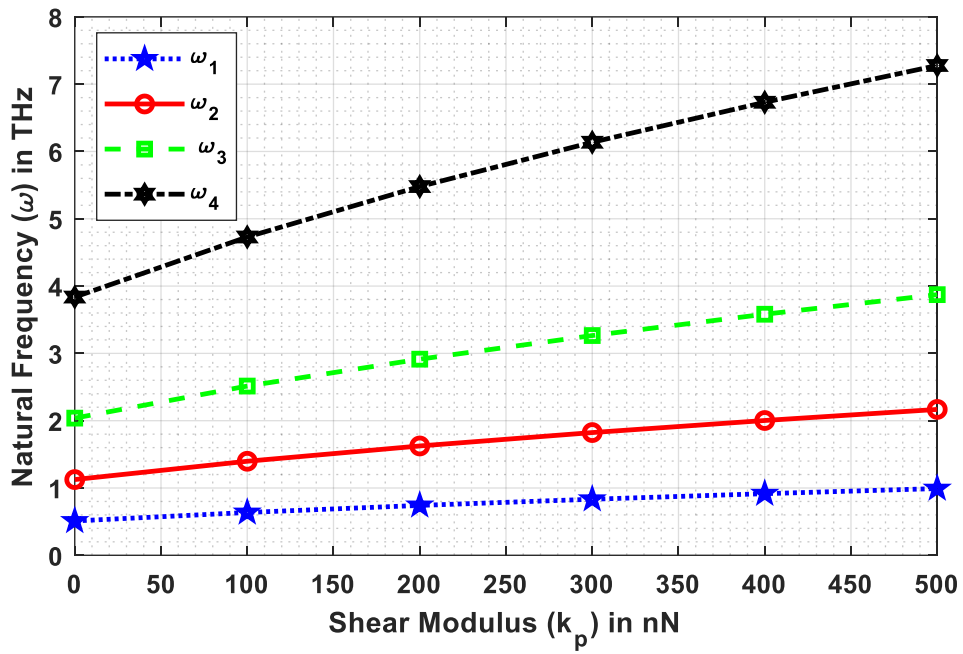| k_p in nN	P_{cr} with $e_0 a = .5$	P_{cr} with $e_0 a = 1$	P_{cr} with $e_0 a = 1.5$	P_{cr} with $e_0 a = 2$
0	188.7128	188.2458	187.5931	186.8733
100	293.2283	292.7612	292.1086	291.3888
200	397.7437	397.2767	396.6240	395.9042
300	502.2592	501.7921	501.1395	500.4197
400	606.7746	606.3076	605.6549	604.9351
500	711.2901	710.8230	710.1704	709.4506

19

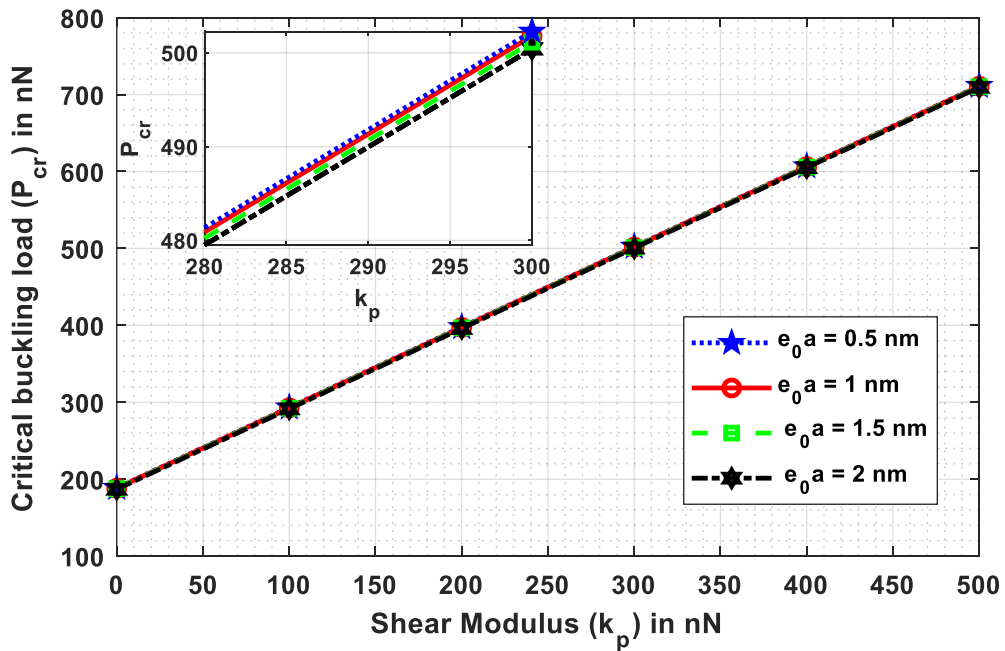**Fig. 7.** Natural frequency Vs. Shear modulus

Fig. 8. Critical buckling load Vs. Shear modulus

20

4.5 Effect of Magnetic field intensity

A parametric study has been carried out to investigate the behaviors of natural frequencies (ω) and critical buckling load (P_{cr}) with respect to axial magnetic field intensity (H_x). For vibration, $L = 10nm$, $e_0 a = 1nm$, $k_w = 1GPa$, and $k_p = 500nN$ are considered by varying H_x from 0 to 1e+9 A/m with an increase of 2e+8 A/m. For this purpose, Table 9 and Fig. 9 are illustrated as numerical and graphical results, respectively. This study reveals that natural frequencies increase with the rise of magnetic field intensity. Likewise, similar study has been conducted for the buckling load. The responses of magnetic field intensity on critical buckling loads are illustrated in Table 10 and Fig. 10 for different values of H_x and k_w. Both the tabular and graphical results show that the critical buckling loads are increasing very rapidly in response to H_x.

Table 9 Natural frequency (ω) in THz with $L = 10nm$, $e_0 a = 1nm$, $k_w = 1GPa$, and $k_p = 500nN$

H_x in A/m	ω_1	ω_2	ω_3	ω_4
0	0.8638	1.8903	3.3830	6.3584
2e+8	0.8974	1.9633	3.5118	6.6001
4e+8	0.9914	2.1674	3.8725	7.2771
6e+8	1.1308	2.4703	4.4087	8.2833
8e+8	1.3012	2.8407	5.0649	9.5149
1e+9	1.4918	3.2555	5.8004	10.8957

Table 10 Critical buckling load (P_{cr}) in nN with with $L = 10nm$, $e_0 a = .5$, and $k_p = 500nN$

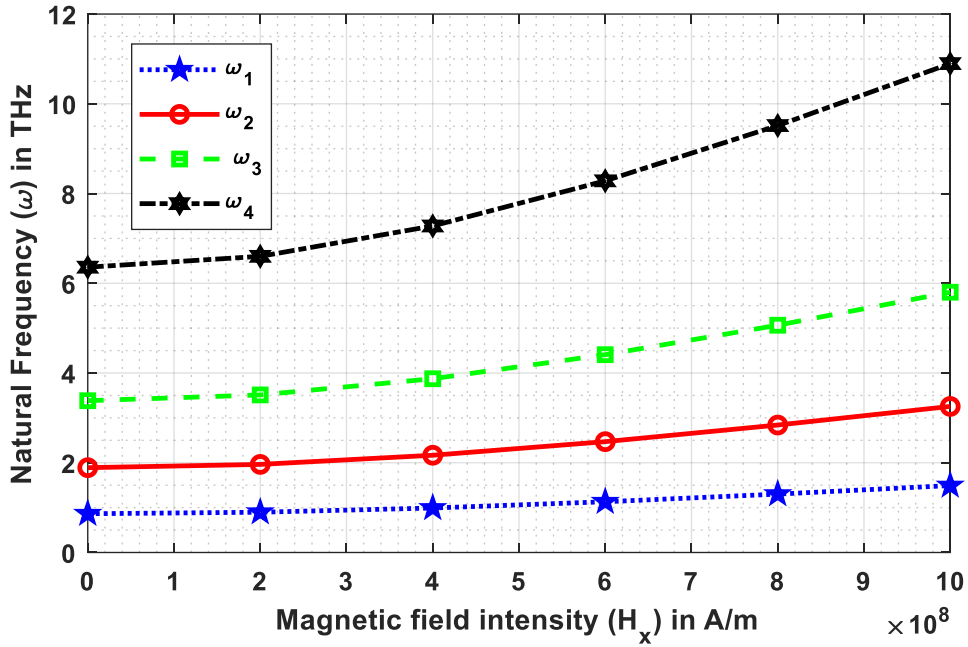| H_x in A/m	P_{cr} with $k_w = 1$	P_{cr} with $k_w = 2$	P_{cr} with $k_w = 3$	P_{cr} with $k_w = 4$
0	540.0991	550.6887	561.2783	571.8680
2e+8	582.8968	593.4864	604.0761	614.6657
4e+8	711.2901	721.8797	732.4693	743.0590
6e+8	925.2788	935.8685	946.4581	957.0477
8e+8	1224.8631	1235.4527	1246.0423	1256.6319
1e+9	1610.0428	1620.6325	1631.2221	1641.8117

Fig. 9. Natural frequency Vs. Magnetic field intensity

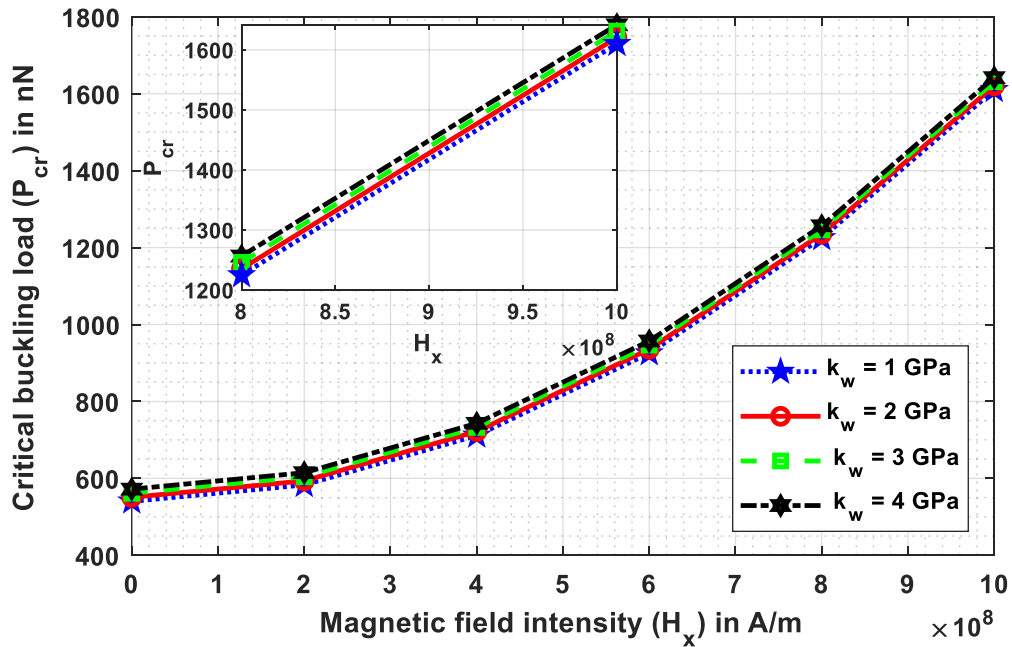**Fig. 10.** Critical buckling load Vs. Magnetic field intensity

22

5. Concluding remarks

A new first-order shear deformation beam theory has been utilized to investigate the vibration and buckling characteristics of nonlocal beam exposed to an axial magnetic field and embedded in Winkler-Pasternak foundation. Von Kármán hypothesis along with Hamilton's principle have been used to develop the governing equations which is solved analytically by implementing Navier's method. Further, natural frequencies and critical buckling loads for Simply Supported (SS) boundary condition are obtained and a parametric study has been carried out to discover the response of various scaling parameters such as small scale parameter, Winkler modulus, shear modulus, and magnetic field intensity on natural frequencies and critical buckling loads. The natural frequencies and critical buckling loads decrease with the increase of nonlocal parameters. Natural frequencies of higher modes are more sensitive towards the nonlocal parameter whereas beam with small sizes possess higher critical buckling loads that exhibit remarkable response towards the small scale effect. Both the natural frequencies and critical buckling loads follow an increasing pattern with the rise of Winkler modulus but this increase is more significant in case of critical buckling load. Likewise, the natural frequencies and buckling loads follow same patters with respect to shear modulus and magnetic field intensity.

References

1. S. Iijima, Nature **354**, 56 (1991).

2. A.R. Juárez, E.C. Anota, H.H. Cocoletzi, J.S. Ramírez, M. Castro, Fuller. Nanotub. Car. N. **25**, 716 (2017).

3. S. Iijima, T. Ichihashi, Nature **363**, 603(1993).

4. T. Murmu, M.A. Mc Carthy, S. Adhikari, J. Sound Vib. **331**, 5069 (2012).

5. K. Kiani, Int. J. Mech. Sci. **87**, 179 (2014).

6. K. Kiani, J. Phys. Chem. Solids **75**, 15 (2014).

23

7. U. Güven, Compos. Struct. **114**, 92 (2014).

8. P. Ponnusamy, A. Amuthalakshmi, Procedia Materials Science **10**, 243 (2015).

9. D.P. Zhang, Y. Lei, Z.B. Shen, Int. J. Mech. Sci. **118**, 219 (2016).

10. M. Hosseini, M. Sadeghi-Goughari, Appl. Math. Model. **40**, 2560 (2016).

11. T.-P. Chang, Compos. Part B-Eng. **114**, 69 (2017).

12. K. Kiani, Comput. Math. Appl. **75**, 3849 (2018).

13. Y.-X. Zhen, S.-L. Wen, Y. Tang, Physica E **105**, 116 (2019).

14. S.C. Pradhan, G.K. Reddy, Comput. Mater. Sci. **50**, 1052 (2011).

15. H. Zeighampour, Y. Tadi Beni, I. Karimipour, Microfluid Nanofluid. **21**, 85 (2017).

16. S. Arghavan, A.V. Singh, J. Sound Vib. **330**, 3102 (2011).

17. Y.Z. Wang, F.M. Li, Mech. Res. Commun. **60**, 45 (2014).

18. M. Rahmanian, M.A. Torkaman-Asadi, R.D. Firouz-Abadi, M.A. Kouchakzadeh, Physica B Condens. Matter. **484**, 83 (2016).

19. R. Fernandes, S. El-Borgi, S.M. Mousavi, J.N. Reddy, A. Mechmoum, Physica E **88**, 18 (2017).

20. M. Malikan, V.B. Nguyen, F. Tornabene, Eng. Sci. Technol. Int J. **21**, 778 (2018).

21. M. Malikan, Sh. Dastjerdi, International Journal of Engineering & Applied Sciences **10**, 21 (2018).

22. M. Malikan, Journal of Applied and Computational Mechanics **5**, 103 (2019).

23. Y.-Z. Wang, Y.-S. Wang, L.-L. Ke, Physica E **83**, 195 (2016).

24. A. Benzair, A. Tounsi, A. Besseghier, H. Heireche, N. Moulay, L. Boumia, J Phys. D Appl. Phys. **41**, 225404 (2008).

25. Y.M. Fu, J.W. Hong, X.Q. Wang, J. Sound Vib. **296**, 746 (2006).

26. J. Jiang, L. Wang, Y. Zhang, Int. J. Mech. Sci. **122**, 156 (2017).

27. M. Malikan, R. Dimitri, F. Tornabene, Compos. Part B-Eng. **158**, 198 (2019).

28. R. Ansari, M. Faghih Shojaei, V. Mohammadi, R. Gholami, H. Rouhi, ZAMM-Journal of Applied Mathematics and Mechanics **95**, 1 (2014).

29. R. Ansari, A. Arjangpay, Physica E **63**, 283 (2014).

30. S.K. Jena, S. Chakraverty, Front. Built Environ. **4**, 63 (2018).

31. S. Chakraverty, S.K. Jena, Curved and Layer. Struct. **5**, 260 (2018).

32. S.K. Jena, S. Chakraverty, F. Tornabene, Mater. Res. Express **6**, 085051 (2019).

33. S.K. Jena, S. Chakraverty, Curved and Layer. Struct. **5**, 201 (2018).

34. S.K. Jena, S. Chakraverty, R.M. Jena, F. Tornabene, Mater. Res. Express **6**, 055016 (2019).

35. S.K. Jena, S. Chakraverty, Curved and Layer. Struct. 6, 68 (2019).

36. S.K. Jena, S. Chakraverty, F. Tornabene, Mater. Res. Express **6**, 0850f2 (2019).

37. R.M. Jena, S. Chakraverty, S.K. Jena, Journal of Applied and Computational Mechanics **5**, 355 (2019).

38. S.K. Jena, S. Chakraverty, Int. J. Comput. Mater. Sci. Eng. **7**, 1850020 (2018).

39. S.K. Jena, S. Chakraverty, F. Tornabene, Nanomaterials **9**, 1326 (2019).

40. S.K. Jena, S. Chakraverty, Curved and Layer. Struct. **6**, 132 (2019).

41. S.K. Jena, S. Chakraverty, R.M. Jena, J. Braz. Soc. Mech. Sci. & Eng. **41**, 436 (2019).

42. M. Malikan, V.B. Nguyen, R. Dimitri, F. Tornabene, Mater. Res. Express **6**, 075041 (2019).

43. O. Civalek, C. Demir, Asian J. Civ. Eng. **12**, 651 (2011).

44. L. Li, Y. Hu, X. Li, Int. J. Mech. Sci. **115**, 135 (2016).

45. R. Barretta, M. Čanadija, F.M. de Sciarra, Arch. Appl. Mech. **86**, 483 (2016).

46. K.G. Eptaimeros, C.C. Koutsoumaris, G.J. Tsamasphyros, Int. J. Mech. Sci. **115**, 68 (2016).

47. O. Rahmani, V. Refaeinejad, S.A.H. Hosseini, Steel Compos. Struct. **23**, pp.339 (2017).

48. B. Akgöz, Ö. Civalek, Compos. Part B-Eng. **129**, 77 (2017).

49. K. Mercan, O. Civalek, Composites Part B **114**, 34 (2017).

50. Ç. Demir, O. Civalek, Int. J. Eng. Sci. **121**, 14 (2017).

51. C. Demir, O. Civalek, Compos. Struct. **168**, 872 (2017).

52. A.M. Zenkour, Eur. Phys. J. Plus **133**, 196 (2018).

53. H.M. Numanoglu, B. Akgöz, O. Civalek, Int. J. Eng. Sci. **130**, 33 (2018).

54. O. Rahmani, M. Shokrnia, H Golmohammadi, S.A.H. Hosseini, Eur. Phys. J. Plus **133**, 42 (2018).

55. M. Dehghan, F. Ebrahimi, Eur. Phys. J. Plus **133**, 466 (2018).

56. V. K. Upadhyayula, S. Deng, M. C. Mitchell, G. B. Smith, Science of the Total Environment **408**, 1 (2009).

57. F. Yu, J. Chen, L. Chen, J. Huai, W. Gong, Z. Yuan, J. Wang, J. Ma, Journal of Colloid and Interface Science **378**, 175 (2012).

58. J. D. Kraus, Electromagnetics, McGraw Hill, USA, 1984.

59. F. Ebrahimi, M.R. Barati, Applied Physics A **123**, 81 (2017).

60. F. Ebrahimi, M. Karimiasl, V. Mahesh, Adv. Nano Res. **7**, 221 (2019).

61. A.C. Eringen, Int. J. Eng. Sci. 10, 1 (1972).

62. Y.X. Zhen, S.L. Wen, Y. Tang, Physica E **105**, 116 (2019).

63. C.M. Wang, Y.Y. Zhang, X.Q. He, Nanotechnology **18**, 105401 (2007).

64. F. Mehralian, Y. Tadi Beni, M. Karimi Zeverdejani, Physica B. **514**, 61 (2017).